

# TWO ALGORITHMS FOR REMOVING OCEAN SURFACE CLUTTER IN MULTISPECTRAL AND HYPERSPECTRAL IMAGES

*Dennis Silva*

*Ron Abileah*

*SRI International*

*333 Ravenswood Avenue*

*Menlo Park, California 94025*

## INTRODUCTION

Two algorithms have been developed by SRI to subtract ocean clutter in multispectral and hyperspectral imagery. The first algorithm employs a physics-based spectral approach to remove glint (referred to here as deglinting). The second algorithm is based on a multichannel, multidimensional pixel-domain whitening algorithm that has been described previously.<sup>1-3</sup>

The two algorithms are compared using a single scene recorded by the AAHIS sensor during an experiment conducted over Kaneohe Bay, Hawaii. We use the scene to demonstrate both the deglinting and whitening operations. With respect to the latter, the pixel-domain whitening operation is followed by a combined spatial-spectral matched filtering operation. The algorithm implementation is unique in that the required signal-whitening operation has been transposed and applied to the data in the form of a “second whitening” operation. The resultant twice-whitened data are then convolved with the unwhitened signal model, eliminating the need to whiten large numbers of signal models either when processing with a bank of matched filters or when spatial nonstationarity (inhomogeneity) forces the partitioning of the image into regions with different statistical properties.

The deglinting algorithm represents a physics-based approach that exploits the spectral difference between solar light reflected from the surface and light scattered from below the surface. This algorithm is particularly interesting, because it is computationally simple and could be implemented in real time at the scan rates normally associated with current push-broom sensors such as AAHIS and HYDICE.

The two algorithms may be used independently or combined to improve detection performance. The latter task of optimally combining the algorithms is one of the objectives of our current research and will be reported in the future. Here, we present the algorithms as independent data conditioning operations. In Section 2, we describe the spectral deglinting algorithm and apply it to the ocean scene mentioned above. In Section 3, we briefly describe the combined spatial-spectral decluttering algorithm, emphasizing the matched-filter processing that has not been reported in detail elsewhere. In Section 4, we summarize our results and describe our plans for future work.

## OCEAN SURFACE CLUTTER REMOVAL (DEGLINTING)

The ability of an optical sensor to look below the surface of the ocean is often complicated by the surface clutter (glint) that arises from specular reflection off wave facets that direct solar light directly into the sensor. A straightforward physics-based deglinting algorithm for removing such clutter is presented in this section. The algorithm exploits the fact that the spectrum of light scattered from beneath the surface is significantly altered by the seawater that it must transit on its way to the sensor. The most important difference occurs in the red portion of the spectrum where absorption effects are most prominent. As a consequence, the light that is reflected from the surface of the ocean has a larger red component than light that has passed through it. The difference is large enough to provide an effective discriminant for isolating the scattered and reflected components of the light entering the sensor.

It is typical to model the light entering a nadir staring sensor as arising from three potential sources given by

$$I(x, y, \lambda) = I^{(u)}(\lambda) + f^{(b)}(x, y)I^{(b)}(\lambda) + f^{(g)}(x, y)I^{(g)}(\lambda), \quad (1)$$

where  $I(x, y, \lambda)$  = total light intensity arriving at sensor (neglecting atmospheric effects)

$I^{(u)}(\lambda)$  = upwelling light intensity

$I^{(b)}(\lambda)$  = back-scattered/reflected light intensity from the sky

$I^{(g)}(\lambda)$  = reflected light intensity from the sun (glint)

$f^{(b)}(x, y)$  = spatial dependence of back-scattered light

$f^{(g)}(x, y)$  = spatial dependence of glint.

This analysis assumes that the field of view of the sensor is small enough to neglect the spatial component of the upwelling light.

Inasmuch as it is difficult to separate the upwelling light from the sky component, we have combined them into a single entity referred to as the scattered light intensity. The resulting model has two components, given by

$$I(x, y, \lambda) \cong f^{(s)}(x, y)I^{(s)}(\lambda) + f^{(g)}(x, y)I^{(g)}(\lambda), \quad (2)$$

with  $f^{(b)}(x, y)I^{(b)}(\lambda) + I^{(u)}(\lambda) \rightarrow f^{(s)}(x, y)I^{(s)}(\lambda)$ . Estimates of  $I^{(s)}(\lambda)$  and  $I^{(g)}(\lambda)$  are obtained from the data under the assumption that the brightest pixels provide the purest examples of glint and the dimmest pixels provide the purest examples of scattered light. The spatial coefficients  $f^{(g)}(x, y)$  and  $f^{(s)}(x, y)$  are then obtained by an error minimization technique and combined with the spectral estimates to produce an estimate of the background for each channel at each pixel location. Deglinted residuals are obtained by subtracting the background estimate from the input image data.

In Figure 1a, we show the data collected by the AAHIS sensor over Kaneohe Bay, Hawaii. This particular image was chosen because of the spatial inhomogeneity that manifests itself as a region of glint in the center. The image data from the AAHIS sensor is normally collected in 70 channels spanning the visible region of the electromagnetic spectrum from 430 to 820 nm. The data were evenly partitioned into 10 channels by integrating neighboring channels into groups of 7. The image presented in Figure 1a is one of the ten spectral channels that were used in the processing. The image spans the blue-green spectral region between 470 and 510 nm. Figure 1b provides the deglinted image derived by subtracting the background estimate for this spectral band. Histograms of the pixel intensities are provided in Figures 2a and 2b. The two extended dark regions are reefs below the surface of the water. Floating above the upper reef there is what appears to be a boat. Just below the boat in the image are five test objects consisting of 4-foot by 4-foot panels of 0.25-inch-thick Plexiglas of varying opacity/transparency. Small opaque blue-colored dots were placed on three transparent panels, with each panel having a different number of dots in order to achieve surface area fill percentages of 12.5%, 25%, and 50%. The remaining two panels consisted of semi-transparent blue Plexiglas with an approximate optical thickness of 25% and 80%, respectively. All five panels were deployed on a coralhead at depths ranging from about 1.5 to 2 meters. A close-up of that portion of the image is provided in Figure 3.

After the application of the deglinting algorithm, the nonuniform pixel intensities of the original image (Figure 1a) give rise to a relatively uniform deep-water background contrasted by the reefs and their structure (Figure 1b). This is also observed in the histograms of Figures 2a and 2b. Here, the broad and somewhat complicated distribution associated with the original pixel intensities is reduced to a bimodal distribution with well-defined, narrow peaks relative to the original image. The left-hand peak is associated with reef pixels, and the right-hand peak is associated with deeper-water pixels.

With the glint mitigated, the target panels in the image are readily visible. The scale of the relief in intensity associated with the man-made objects is provided in the form of three-dimensional plots.

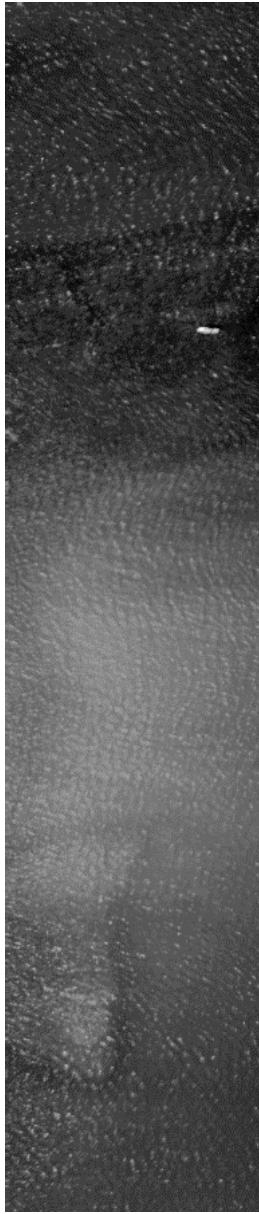


*Figure 1a. Original scene recorded by AAHIS sensor in the 470 to 510 nm band.*

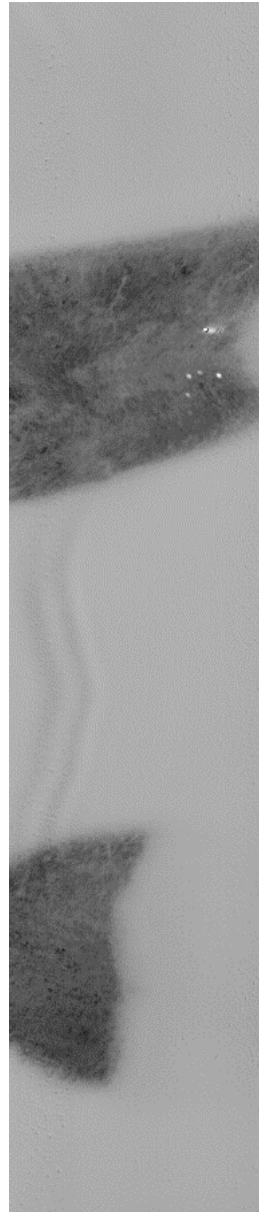


*Figure 1b. Deglinted residuals in the 470 to 510 nm band.*

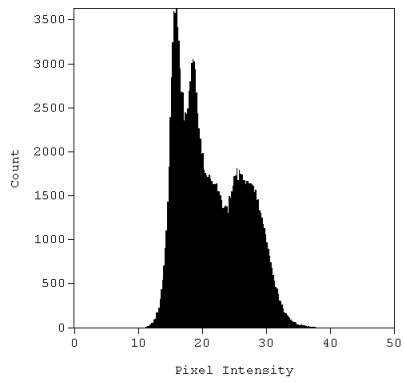


Figure 2a. Histogram of original image in the 470 to 510 nm band.

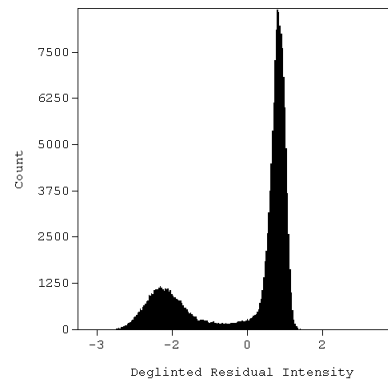


Figure 2b. Histogram of deglintered residuals in the 470 to 510 nm band.

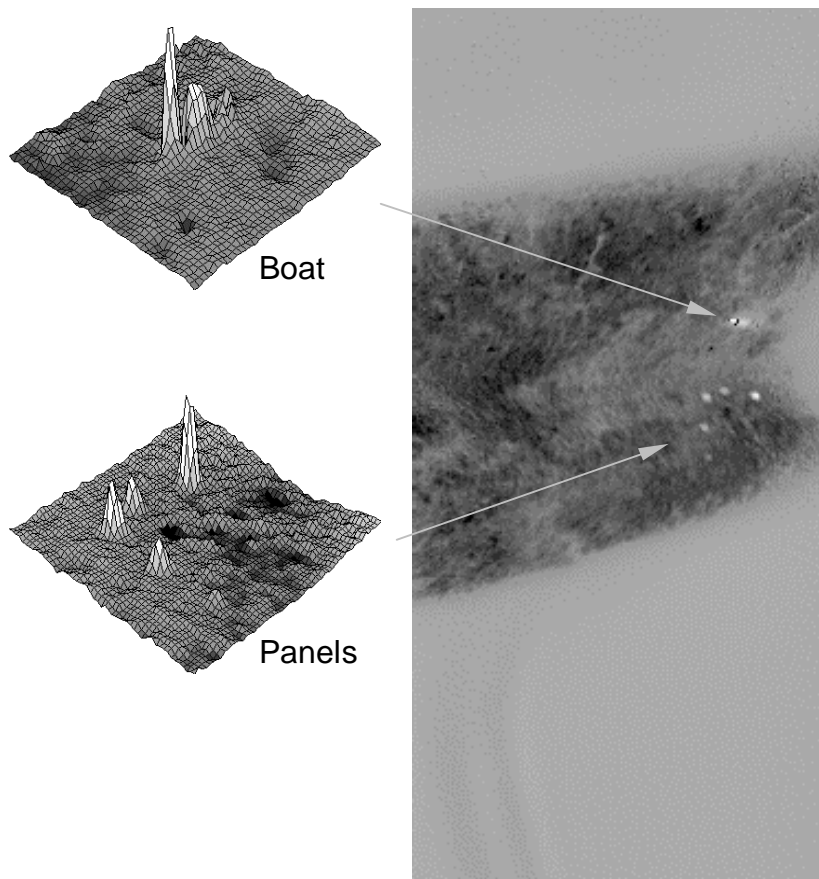


Figure 3. Close-up of region in the deglintered image containing nonbackground features.

## SIMULTANEOUS SPATIAL-SPECTRAL DECLUTTERING

For matched-filter processing in the presence of multichannel correlated background statistics, both spatial and spectral decluttering must be employed if the conditions for optimal performance are to be met. The statistical approach developed by SRI models the correlation in space and spectral channel with a linear predictive filter. For processing image cubes of the type produced by push-broom sensors such as HYDICE and AAHIS, we represent the intensity of each pixel as a linear combination of pixel intensities associated with neighboring pixels in the same channel as well as all other channels. The estimation neighborhood of each pixel is taken to be a causal support space of finite extent in the spatial dimension spanning all of the channels. The filter coefficients are obtained from the data via least squares by way of a multichannel formulation of the Yule-Walker equations. Subtracting the estimates of the background pixel intensities from the input pixel intensities of the original image yields the whitened residuals. From previous work,<sup>1-3</sup> the residuals  $\underline{Z}$  are derived from the input data  $\underline{X}$  by evaluating the vector-notation expression

$$\underline{Z} = \sqrt{\Lambda_Z^{-1}}(I - \Phi)\underline{X}, \quad (3)$$

where  $\Phi$  represents the filter coefficients that constitute the whitening kernel,  $I$  is the identity matrix, and  $\Lambda$  is the zero-lag cross-channel covariance matrix estimated from the background-subtracted residuals  $(I - \Phi)\underline{X}$ . In more formal algebraic notation,

Equation 3 is given by

$$Z_l(i, j) = \sqrt{\Lambda_Z^{-1}} \left( X_l(i, j) - \sum_{l'=1}^M \sum_{i', j' \in S} \Phi_{ll'}(i', j') X_{l'}(i - i', j - j') \right), \quad (4)$$

where  $l$  labels the channel,  $i$  and  $j$  label the spatial indices, and  $S$  represents the  $n \times m$  spatial support space of the filter given by

$$S = \{(i', j'): 0 < i' \leq n, -m \leq j' \leq m\} \cup \{(i', j'): i' = 0, 1 \leq j' \leq m\}, \quad (5)$$

Matched-filter processing consists of convolving a whitened signal model with the whitened residual values obtained by way of Equation 3, above:

$$\left( \sqrt{\Lambda_Z^{-1}}(I - \Phi)\underline{S} \right)^T \otimes \left( \sqrt{\Lambda_Z^{-1}}(I - \Phi)\underline{X} \right), \quad (6)$$

Alternatively, Equation 6 may be rewritten so that both whitening operations are performed on the data:

$$\underline{S}^T \otimes (I - \Phi)^T \Lambda_Z^{-1} (I - \Phi)\underline{X}. \quad (7)$$

The latter formulation has the practical advantage that the “twice-whitening” operation on the data need only be performed once and is valid for any signal model. This convenience is particularly valuable when testing multiple signal hypotheses or processing images with nonstationary spatial statistics that require partitioning the image into segments requiring multiple convolution kernels.

In Figures 4a and 4b, the matched-filter detection approach of Equation 7 was applied to the same set of data used in Section 2. As before, the 70-channel spectrum was partitioned into 10 processing bins of 7 channels each. In this example, a surrogate filter was used to approximate an appropriate matched filter. Since the tagged panels were blue in color, the signal model was tuned to detect background anomalies in the first two channels covering the spectral range from 430 to 510 nm. The channel weights used were (1,1,0,0,0,0,0,0,0,0). Spatially, the convolution kernel consisted of a  $3 \times 3$  matrix of values

$$\begin{pmatrix} 0.25 & 0.50 & .025 \\ 0.50 & 1.0 & 0.50 \\ 0.25 & 0.50 & 0.25 \end{pmatrix}$$

where the same weights were used for each spectral channel.

Comparing Figure 4 with Figure 3, we see that the latter has gone a long way toward removing all of the naturally occurring background clutter and leaving only the man-made objects as background anomalies. In addition, the signal filter, which was designed to approximate the spatial and spectral properties of the target panels, is seen to emphasize these image elements over other potential man-made image elements such as the boat.

## SUMMARY

We have presented two algorithms for conditioning multichannel imagery: a physics-based algorithm that exploits the spectral properties of glint in order to remove it, and a more comprehensive statistics-based algorithm that attempts to remove all background clutter. The deglinting algorithm has the advantage of being computationally simple, making it a good candidate for real-time processing. For simple backgrounds it can serve as a conditioner for matched filtering. In contrast, the clutter-removal algorithm is more computationally expensive, but it is robust enough to condition relatively complicated backgrounds for match-filter processing.

The algorithms may be used independently or in combination. Here, we have treated them as stand-alone processes. Future work will emphasize their use in combination. For example, the deglinting operation resulted in a bimodal distribution that could be used to partition the sample image into water data and reef data. Using data from the central regions of the two distributions, independent estimates of the whitening kernels for water pixels and reef pixels can be made and applied to the corresponding

image segments. Current work is addressing the issues associated with image segmentation in support of the development of an omnibus algorithm capable of removing optical background clutter in any ocean environment.

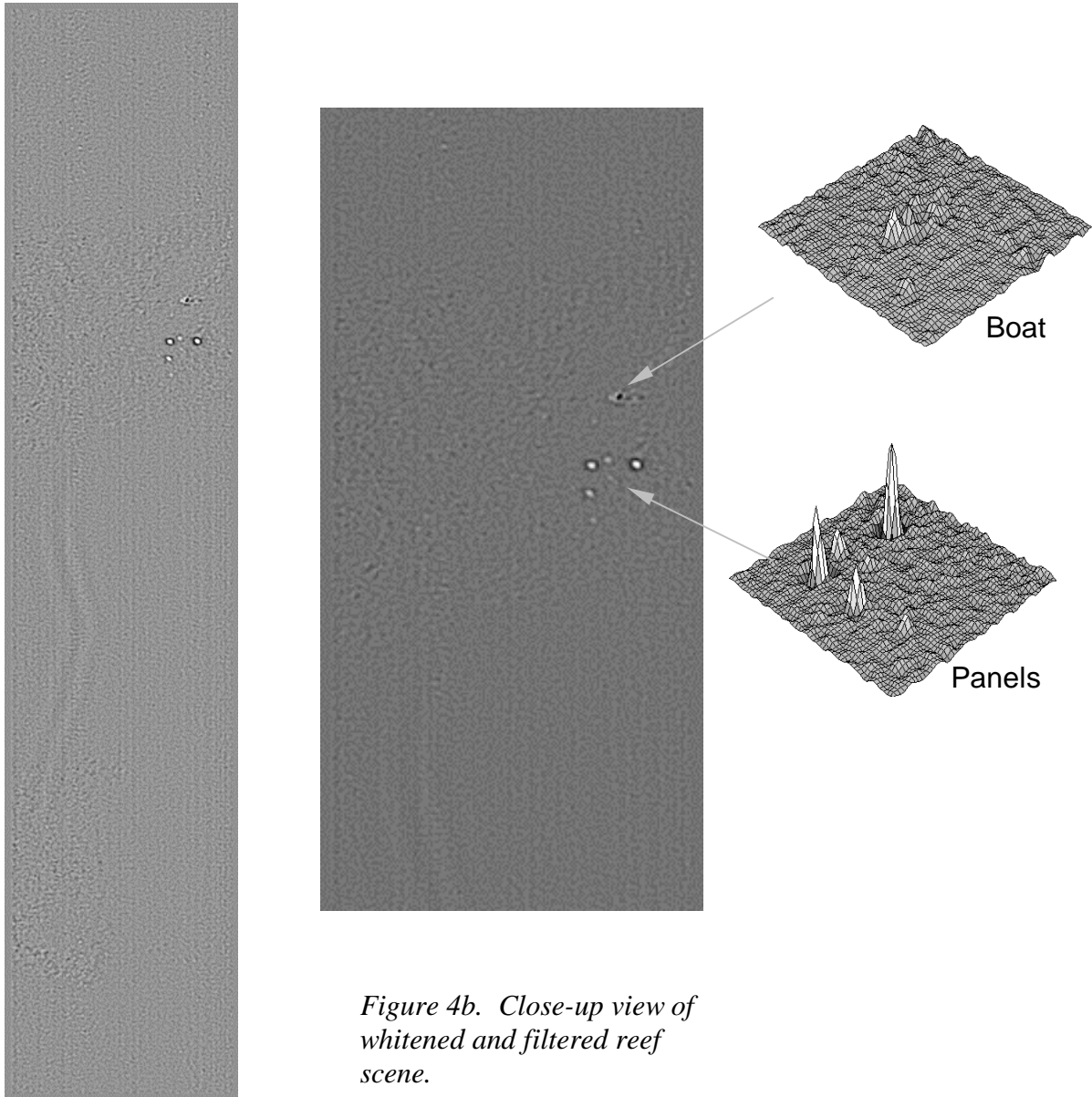


*Figure 4a. Reef scene whitened and filtered.*

*Figure 4b. Close-up view of whitened and filtered reef scene.*

## ACKNOWLEDGMENTS

This paper reports on research conducted at SRI International over the last few years. The authors would like to acknowledge the contribution of Russell Warren who provided the preliminary mathematical foundation for this effort.

## REFERENCES

1. D. Silva, I. Abdou, and R. Warren, "Optimum detection of small targets in a cluttered background," *Opt. Eng.* **37**, 83–92 (1998).
2. D. Silva, R. Warren, and J. Little, "Multichannel, time-dependent whitening of non-Gaussian data for weak-signal image processing," in *Signal and Data Processing of Small Targets 1994*, O. E. Drummond, Ed., *Proc. SPIE* **2235**, 14–27 (1994).
3. D. Silva and R. Warren, "Multichannel detection of small targets in Gaussian and non-Gaussian clutter," in *Signal and Data Processing of Small Targets 1995*, O. E. Drummond, Ed., *Proc. SPIE* **2561**, 112–123 (1995).